Available online at www.sciencedirect.com
ScienceDirect
Magnetic Resonance Imaging 29 (2011) 126–131
MAGNETIC RESONANCE IMAGING

# Numerical solutions to the time-dependent Bloch equations revisited

Kenya Murase*, Nobuyoshi Tanki

*Department of Medical Physics and Engineering, Division of Medical Technology and Science, Faculty of Health Science, Graduate School of Medicine, Osaka University, Osaka 565-0871, Japan*

Received 30 May 2010; revised 19 July 2010; accepted 26 July 2010

**Abstract**

The purpose of this study was to demonstrate a simple and fast method for solving the time-dependent Bloch equations. First, the time-dependent Bloch equations were reduced to a homogeneous linear differential equation, and then a simple equation was derived to solve it using a matrix operation. The validity of this method was investigated by comparing with the analytical solutions in the case of constant radiofrequency irradiation. There was a good agreement between them, indicating the validity of this method. As a further example, this method was applied to the time-dependent Bloch equations in the two-pool exchange model for chemical exchange saturation transfer (CEST) or amide proton transfer (APT) magnetic resonance imaging (MRI), and the Z-spectra and asymmetry spectra were calculated from their solutions. They were also calculated using the fourth/fifth-order Runge-Kutta-Fehlberg (RKF) method for comparison. There was also a good agreement between them, and this method was much faster than the RKF method. In conclusion, this method will be useful for analyzing the complex CEST or APT contrast mechanism and/or investigating the optimal conditions for CEST or APT MRI.


*Keywords:* Bloch equations; Analytical solution; Numerical solution; CEST MRI; APT MRI

## 1. Introduction

Chemical exchange saturation transfer (CEST) is a novel contrast mechanism for magnetic resonance imaging (MRI) [1] and has been increasingly used to detect dilute proteins via the interaction between labile solute protons and bulk water protons [2–4]. Moreover, amide proton transfer (APT) imaging, a particular type of CEST MRI that specifically probes labile amide protons of endogenous mobile proteins and peptides in tissue, has been explored for imaging diseases such as tumor and acute stroke [5,6] and is currently under intensive evaluation for clinical translation. However, CEST or APT MRI contrast mechanism is complex, depending not only on the concentration of CEST agents or amide protons, exchange and relaxation properties, but also varying with experimental conditions such as magnetic field strength and radiofrequency (RF) power [7]. Thus, for investigating these optimal conditions, numerical simulations are useful and effective [8]. To perform extensive numerical simulations for CEST or APT MRI, it will be necessary to develop a simple and fast method for obtaining the numerical solutions to the time-dependent Bloch equations.

The Bloch equations have been solved by application of a Laplace transform [9,10], a multiple-derivative method [11] and numerical integration [12]. In most cases, however, the solutions have been given for various limiting situations, such as steady-state solutions [13], on-resonance solutions [14], solutions neglecting relaxation [12] and those that involve weak RF fields [15].

The purpose of this study was to demonstrate a simple and fast method for solving the time-dependent Bloch equations and to validate this method by comparing with analytical solutions or other numerical solutions.

## 2. Materials and methods

### 2.1. Bloch equations in the case of constant RF irradiation

The time-dependent Bloch equations for constant RF irradiation in the absence of diffusion can be given by [16]

$$\begin{cases} \dfrac{dM_x}{dt} = \Delta\omega M_y(t) - R_2 M_x(t) \\ \dfrac{dM_y}{dt} = -\Delta\omega M_x(t) - R_2 M_y(t) + \omega_1 M_z(t), \\ \dfrac{dM_z}{dt} = -\omega_1 M_y(t) - R_1\left[M_z(t) - M_z^0\right] \end{cases} \quad (1)$$

* Corresponding author. Tel.: +81 6 6879 2571; fax: +81 6 6879 2571.
*E-mail address:* murase@sahs.med.osaka-u.ac.jp (K. Murase).

0730-725X/$ – see front matter © 2011 Elsevier Inc. All rights reserved.
doi:10.1016/j.mri.2010.07.003

where $M_x(t)$, $M_y(t)$ and $M_z(t)$ denote the $x$, $y$ and $z$ components of the magnetization in the rotating frame at time $t$, respectively; $\omega_1$, the nutation rate of the RF irradiation with a frequency of $\omega$ applied along the $x$-axis of the rotating frame (=$\gamma B_1$, where $\gamma$ and $B_1$ are the gyromagnetic ratio and RF power, respectively) and $\Delta\omega$ (=$\omega_0-\omega$), the offset frequency of the RF irradiation with respect to the Larmor frequency ($\omega_0$). $R_1$ and $R_2$ denote the relaxation rates, i.e., the reciprocals of the longitudinal ($T_1$) and transverse relaxation times ($T_2$), respectively. $M_z^0$ denotes the thermal equilibrium z magnetization in the absence of RF irradiation.

The differential equations given by Eq. (1) can be combined into one vector equation (homogeneous linear differential equation):

$$\frac{d\mathbf{M}}{dt} = \mathbf{A}\cdot\mathbf{M}, \tag{2}$$

where

$$\mathbf{M} = \begin{bmatrix} M_x(t) & M_y(t) & M_z(t) & 1 \end{bmatrix}^T \tag{3}$$

and

$$\mathbf{A} = \begin{pmatrix} -R_2 & \Delta\omega & 0 & 0 \\ -\Delta\omega & -R_2 & \omega_1 & 0 \\ 0 & -\omega_1 & -R_1 & R_1M_z^0 \\ 0 & 0 & 0 & 0 \end{pmatrix}. \tag{4}$$

$T$ in Eq. (3) denotes the matrix transpose.

The solution of Eq. (2) can be given by

$$\mathbf{M}(t) = e^{\mathbf{A}t}\mathbf{M}(0), \tag{5}$$

where $\mathbf{M}(0)$ is the matrix of initial values at $t$=0. $e^{\mathbf{A}t}$ is the matrix exponential, which can be given by (see Appendix A)

$$e^{\mathbf{A}t} = \mathbf{T}e^{\mathbf{D}t}\mathbf{T}^{-1} = \mathbf{T}diag\left[e^{\lambda_1 t}, e^{\lambda_2 t}, e^{\lambda_3 t}, e^{\lambda_4 t}\right]\mathbf{T}^{-1}, \tag{6}$$

where $\mathbf{T}$ is the matrix of eigenvectors (eigenmatrix) for $\mathbf{A}$, and $\lambda_1$, $\lambda_2$, $\lambda_3$ and $\lambda_4$ are their eigenvalues. It should be noted that the last eigenvalue, i.e., $\lambda_4$ is always zero.

### 2.2. Comparison with analytical solution

The analytical solution in the case of constant RF irradiation has been given by Mulkern and Williams [9] (see Appendix B). To validate the solution given by Eq. (5), we compared it with the analytical solution given by Mulkern and Williams [9] under the following conditions: $R_1$=1 $s^{-1}$, $\Delta\omega$ =2500 Hz, $\omega_1$=150 Hz, $M_z^0$=1, $\mathbf{M}(0)$=[0 0 1 1]$^T$ and $R_2$ was varied as 50, 200 and 1000 $s^{-1}$.

### 2.3. Bloch equations in the two-pool exchange model for CEST or APT MRI

The time-dependent Bloch equations in the two-pool exchange model for CEST or APT MRI are given by [8]

$$\begin{cases} \frac{dM_x^a}{dt} = \Delta\omega_a M_y^a(t) - R_2^a M_x^a(t) - k_a M_x^a(t) + k_b M_x^b(t) \\ \frac{dM_x^b}{dt} = \Delta\omega_b M_y^b(t) - R_2^b M_x^b(t) - k_b M_x^b(t) + k_a M_x^a(t) \\ \frac{dM_y^a}{dt} = -\Delta\omega_a M_x^a(t) - R_2^a M_y^a(t) - k_a M_y^a(t) + k_b M_y^b(t) + \omega_1 M_z^a(t) \\ \frac{dM_y^b}{dt} = -\Delta\omega_b M_x^b(t) - R_2^b M_y^b(t) - k_b M_y^b(t) + k_a M_y^a(t) + \omega_1 M_z^b(t) \\ \frac{dM_z^a}{dt} = -\omega_1 M_y^a(t) - R_1^a\left[M_z^a(t) - M_0^a\right] - k_a M_z^a(t) + k_b M_z^b(t) \\ \frac{dM_z^b}{dt} = -\omega_1 M_y^b(t) - R_1^b\left[M_z^b(t) - M_0^b\right] - k_b M_z^b(t) + k_a M_z^a(t) \end{cases}, \tag{7}$$

where superscripts $a$ and $b$ show the parameters in pool a and pool b, respectively. For example, $M_x^a(t)$ denotes the x component of the magnetization in pool a at time $t$. $k_a$ denotes the exchange rate from spins in pool a to those in pool b, while $k_b$ denotes that from spins in pool b to those in pool a. $M_0^a$ and $M_0^b$ denote the thermal equilibrium z magnetizations in pool a and pool b, respectively. $\Delta\omega_a$ and $\Delta\omega_b$ are given by $\omega_a-\omega$ and $\omega_b-\omega$, respectively, where $\omega_a$ and $\omega_b$ are the Larmor frequencies in pool a and pool b, respectively, and $\omega$ is the frequency of RF irradiation. In this case, $\mathbf{M}$ and $\mathbf{A}$ in Eq. (2) are given by

$$\mathbf{M} = \begin{bmatrix} M_x^a(t) & M_x^b(t) & M_y^a(t) & M_y^b(t) & M_z^a(t) & M_z^b(t) & 1 \end{bmatrix}^T \tag{8}$$

and

$$\mathbf{A} = \begin{pmatrix} -(R_2^a + k_a) & k_b & \Delta\omega_a & 0 & 0 & 0 & 0 \\ k_a & -(R_2^b + k_b) & 0 & \Delta\omega_b & 0 & 0 & 0 \\ -\Delta\omega_a & 0 & -(R_2^a + k_a) & k_b & \omega_1 & 0 & 0 \\ 0 & -\Delta\omega_b & k_a & -(R_2^b + k_b) & 0 & \omega_1 & 0 \\ 0 & 0 & -\omega_1 & 0 & -(R_1^a + k_a) & k_b & R_1^a M_0^a \\ 0 & 0 & 0 & -\omega_1 & k_a & -(R_1^b + k_b) & R_1^b M_0^b \\ 0 & 0 & 0 & 0 & 0 & 0 & 0 \end{pmatrix}. \tag{9}$$

As an illustrative example, CEST or APT MRI was numerically simulated using the two-pool exchange model consisting of bulk water (pool a) and labile protons (pool b). A chemical offset of 700 Hz was chosen for simulation as done by Sun [7] as it represents the frequency offset of ensemble amide proton from endogenous proteins and peptides, observed at 4.7 T. Typical longitudinal and transverse relaxation times for bulk water ($T_1^a$=3 s and $T_2^a$=2 s) and labile protons ($T_1^b$=770 ms and $T_2^b$=33 ms) were used [17]. The exchange rate from labile protons to bulk water ($k_b$) was assumed to be 200 $s^{-1}$, while that from bulk water to labile protons ($k_a$) was calculated from the following relationship based on the mass balance between two pools [8]: $k^a=(M_0^b/M_0^a)k_b$. The labile proton concentration with respect to bulk water proton ($M_0^b/M_0^a$) was assumed to be 0.001. The RF power ($B_1$) was varied as 1 μT ($\omega_1$=42.6 Hz), 2 μT ($\omega_1$=85.2 Hz) and 3 μT ($\omega_1$=127.7 Hz). It should be

noted that $\omega_1$ is given by $\omega_1=\gamma \boldsymbol{B}_1$ as previously described, where $\gamma$ is 42.58 MHz/T.

The CEST effect has usually been analyzed using the so-called Z-spectra and asymmetry spectra (A-spectra) [17]. Thus, we calculated these spectra as a function of time by using the following equations:

$$\mathrm{Z-spectra} = \frac{M_z^{\mathrm{a}}(\Delta\omega_{\mathrm{a}})}{M_0^{\mathrm{a}}} \tag{10}$$

and

$$\mathrm{A-spectra} = \frac{M_z^{\mathrm{a}}(-\Delta\omega_{\mathrm{a}}) - M_z^{\mathrm{a}}(\Delta\omega_{\mathrm{a}})}{M_0^{\mathrm{a}}}, \tag{11}$$

where $M_z^{\mathrm{a}}(\Delta\omega_a)$ denotes the z magnetization of pool a (bulk water) with saturation at $\Delta\omega_a$. In this study, $\Delta\omega_a$ was varied from −1000 Hz to 1000 Hz with an interval of 10 Hz.

We also solved the Bloch equations given by Eq. (7) and calculated the above spectra by using the fourth/fifth-order Runge-Kutta-Fehlberg (RKF) algorithm [18] (ode45 in MatLab; The MathWorks, Natick, MA, USA) with an absolute error tolerance for each integration step of $10^{-6}$, and compared with the results obtained by our method [Eq. (5)].

Calculations were performed using MatLab on Intel Core i7 CPU (3.2 GHz) with 6-GB RAM.

## 3. Results

Fig. 1 shows the comparison between the numerical and analytical solutions in the case of constant RF irradiation. Fig. 1A, B, and C show the $x$, $y$ and $z$ components of magnetization, respectively. The solid, dashed and dotted lines show the numerical solutions obtained by Eq. (5) for $R_2$ of 50, 200 and 1000 $s^{-1}$, respectively, while the closed circles, squares and triangles show the analytical solutions shown in Appendix B. Note that the analytical solutions are shown at an interval of 0.1 s to simplify the graphs. As shown in Fig. 1, there were good agreements between them.

Fig. 2 shows the Z-spectra [Eq. (10)] and A-spectra [Eq. (11)] obtained by Eq. (5) and those obtained using the RKF algorithm for the two-pool exchange model. Fig. 2A, B, and C show the results at 2.5 s, 5 s and 10 s, respectively. The solid, dashed and dotted lines show the results obtained by Eq. (5) for $B_1$ of 1, 2 and 3 μT, respectively, while the closed circles, squares and triangles show those obtained using the RKF algorithm for $B_1$ of 1, 2 and 3 μT, respectively. Note that the results obtained by the RKF algorithm are shown at an interval of 100 Hz to simplify the graphs. As shown in Fig. 2, there were good agreements between the results obtained by the two methods.

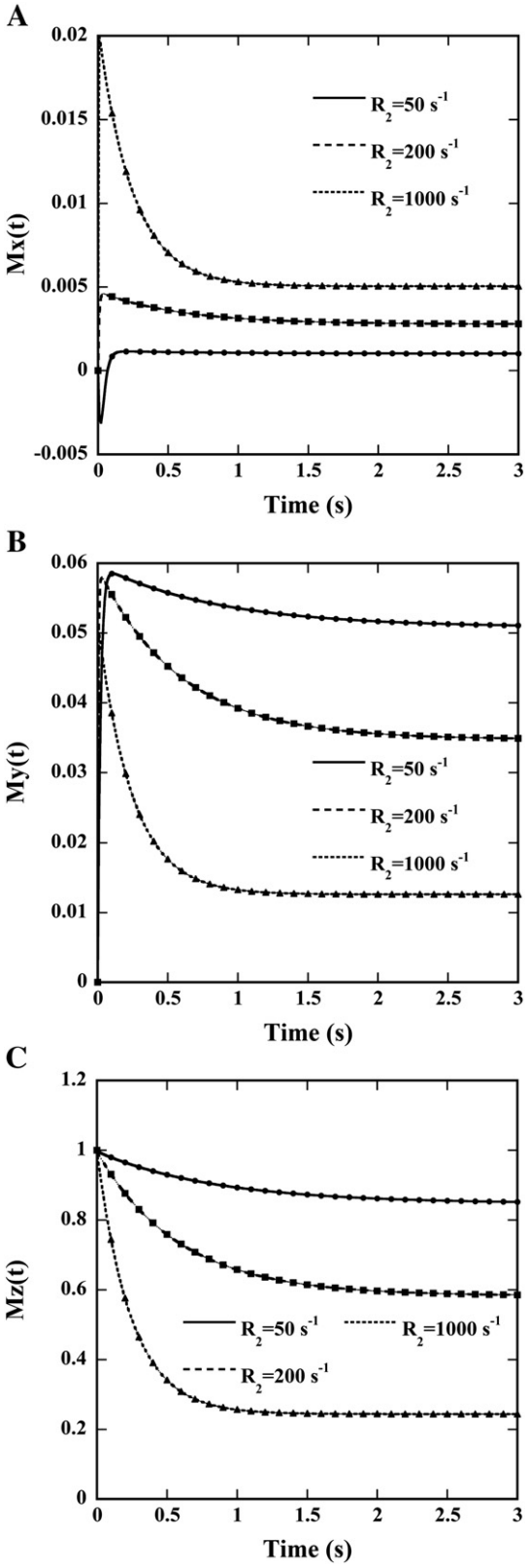


Fig. 1. Magnetization in the rotating frame as a function of time for various transverse relaxation rates ($R_2$) in the case of constant radiofrequency (RF) irradiation. Panels (a), (b) and (c) show the $x$, $y$ and $z$ components, respectively. The solid, dashed and dotted lines show the numerical solutions obtained by Eq. (5) for $R_2$ of 50, 200 and 1000 $s^{-1}$, respectively, while the closed circles, squares and triangles show the analytical solutions shown in Appendix B for $R_2$ of 50, 200 and 1000 $s^{-1}$, respectively. Note that the closed circles, squares and triangles are shown at an interval of 0.1 s to simplify the graphs.

Regarding computation time, it took about 0.018 s for our method [Eq. (5)] to obtain the results shown in Fig. 2A, whereas it took about 93.7 s for the RKF algorithm, indicating that our method was faster than the method using the RKF algorithm by a factor of approximately 5200.

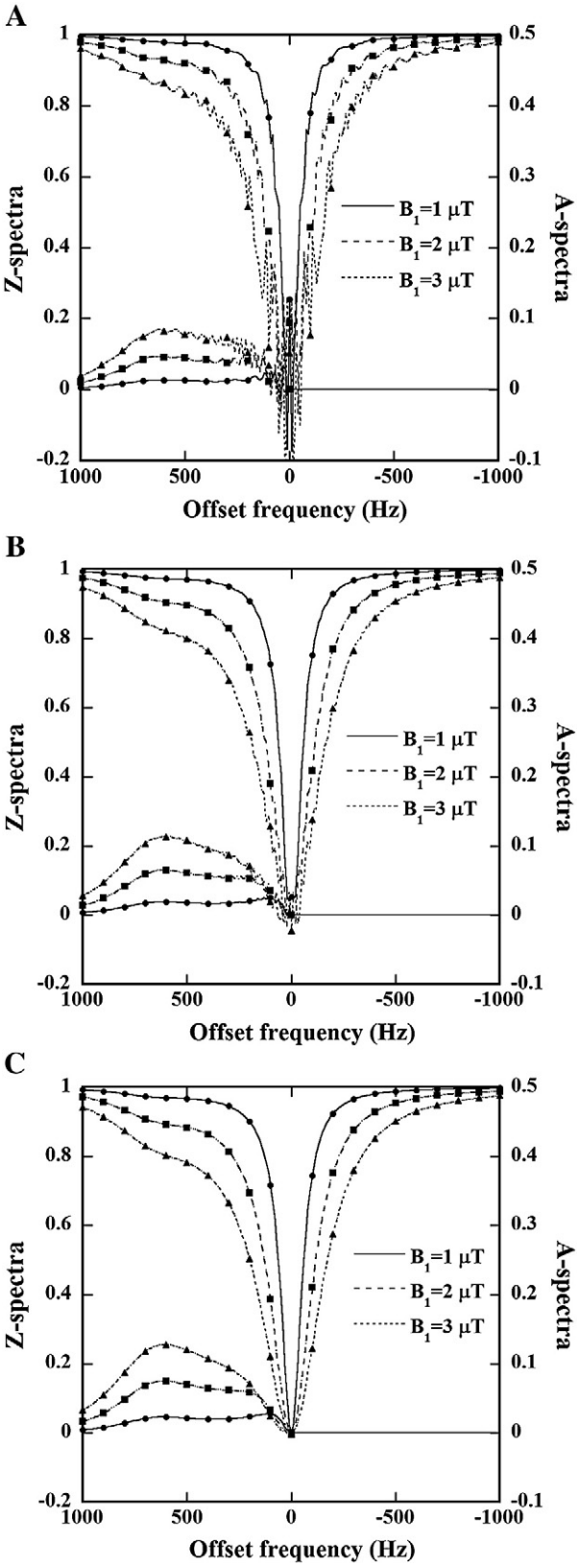


Fig. 2. Z-spectra (middle) and asymmetry spectra (A-spectra) (lower left) calculated from Eqs. (10) and (11), respectively, for various RF powers ($B_1$) in the case of the two-pool exchange model for chemical exchange saturation transfer or amide proton transfer magnetic resonance imaging. Panels (a), (b) and (c) show the results at 2.5, 5 and 10 s, respectively. The solid, dashed and dotted lines show the numerical solutions obtained by Eq. (5) for $B_1$ of 1, 2 and 3 μT, respectively, while the closed circles, squares and triangles show those obtained using the fourth/fifth-order Runge-Kutta-Fehlberg algorithm for $B_1$ of 1, 2 and 3 μT, respectively. Note that the closed circles, squares and triangles are shown at an interval of 100 Hz to simplify the graphs.

## 4. Discussion

In this study, we derived a simple equation for solving the time-dependent Bloch equations using a matrix operation [Eqs. (2) and (5)]. As shown in Fig. 1, the numerical solutions obtained by our method agreed with the analytical solutions [9]. The analytical solutions given by Mulkern and Williams [9] appear to be effective for investigating the validity of these numerical solutions. We also compared the Z- and A-spectra obtained by our method for the two-pool exchange model in CEST or APT MRI with those obtained using the RKF algorithm. There was also a good agreement between them (Fig. 2). These results appear to indicate the validity of our method.

For calculating the solutions to the time-dependent Bloch equations using Eq. (5), most computation time is spent to calculate the eigenvectors and eigenvalues of matrix **A**. However, it is necessary to carry out this calculation only once regardless of $t$ in Eq. (5). As previously described, the matrix exponential was computed using diagonalization in this study. Besides this approach, the matrix exponential can also be computed using a scaling and squaring algorithm with Pade approximation [19]. This approximation has been used in the function supplied in MatLab (expm). Although there was a good agreement between the results obtained by the two methods (data not shown), our method was faster than the method using the Pade approximation by a factor of approximately 2.

In this study, the nutation rate of the RF pulse ($\omega_1$) was assumed to be constant. However, without loss of generality, the time-varying nutation rate of the RF pulse can be adequately approximated by a rectangular pulse with the same root-mean-square power [20]:

$$\omega_1 = \gamma\left(\frac{\int_0^{\Delta t} B_1^2(\tau)d\tau}{\Delta t}\right)^{\frac{1}{2}}, \tag{12}$$

where $\Delta t$ is the duration of the RF irradiation. Thus, our method can also be applied to the case with the time-varying nutation rate of the RF pulse, by using Eq. (12).

Numerical solutions to the time-dependent Bloch equations including direct saturation can also be solved using an ordinary differential equation solver such as ode45 in

MatLab. We compared the numerical solutions obtained by our method and those obtained by the ordinary differential equation solver. As previously described, the computation time was considerably reduced when using our method [Eq. (5)] (by a factor of approximately 5200 in this study). Thus, our method can be included in the nonlinear least-squares fitting routine to calculate the parameters such as the transition rate or lifetime of CEST agents [7].

In this study, we used the two-pool exchange model for CEST or APT MRI as an illustrative example. As pointed out by Woessner et al. [8], paramagnetic CEST agents often have more than one type of exchangeable proton. For such cases, it is necessary to expand the Bloch equations to multi-pool exchange models. Our method can be easily extended to multi-pool models by modifying the matrix **A** in Eq. (5).

In conclusion, we presented a simple and fast numerical method for solving the time-dependent Bloch equations and confirmed its validity by comparing with analytical or other numerical solutions. Our method will be useful for analyzing the complex CEST or APT contrast mechanism and/or for investigating the optimal conditions for CEST or APT MRI.

## Appendix A

The matrix exponential $e^{\mathbf{A}t}$ is represented by the Maclaurin series as

$$e^{\mathbf{A}t} = \sum_{k=0}^{\infty} \frac{\mathbf{A}^k t^k}{k!}. \tag{A1}$$

In general, this summation is difficult to compute because of the tediousness of calculating repeated powers of $\mathbf{A}^k$. However, there are some shortcuts that we can use. One of the shortcuts is diagonalization. If matrix **A** has a full set of eigenvectors, then **A** is diagonalizable:

$$\mathbf{T}^{-1}\mathbf{A}\mathbf{T} = \mathbf{D} \text{ or } \mathbf{A} = \mathbf{T}\mathbf{D}\mathbf{T}^{-1}, \tag{A2}$$

where **T** is the matrix of eigenvectors (eigenmatrix) and **D** is the diagonal matrix given by

$$\mathbf{D} = \mathrm{diag}[\lambda_1,\ \lambda_2,\ \ldots,\ \lambda_n], \tag{A3}$$

with $\lambda_1$, $\lambda_2$, ..., $\lambda_n$ being eigenvalues. Substituting Eq. (A2) into Eq. (A1) yields

$$\begin{aligned} e^{\mathbf{A}t} &= \sum_{k=0}^{\infty} \frac{(\mathbf{T}\mathbf{D}\mathbf{T}^{-1})^k t^k}{k!} = \mathbf{T}\sum_{k=0}^{\infty} \frac{\mathbf{D}^k t^k}{k!}\mathbf{T}^{-1} \\ &= \mathbf{T}\mathrm{diag}\left[\sum_{k=0}^{\infty} \frac{{\lambda_1}^k t^k}{k!}, \sum_{k=0}^{\infty} \frac{{\lambda_2}^k t^k}{k!}, \cdots, \sum_{k=0}^{\infty} \frac{{\lambda_n}^k t^k}{k!}\right]\mathbf{T}^{-1}. \\ &= \mathbf{T}\mathrm{diag}\left[e^{\lambda_1 t},\ e^{\lambda_2 t},\ \ldots,\ e^{\lambda_n t}\right]\mathbf{T}^{-1} \end{aligned} \tag{A4}$$

## Appendix B

When constant RF irradiation and $M_x(0)=M_y(0)=0$ and $M_z(0)=1$ were assumed, the analytical solutions for $M_x(t)$, $M_y(t)$ and $M_z(t)$ are given as follows [10]:

$$M_x(t) = g_x^{ss} + g_1 e^{\alpha_1 t} + g_2 e^{\alpha_2 t} + g_3 e^{\alpha_3 t}, \tag{B1}$$

$$M_y(t) = f_x^{ss} + f_1 e^{\alpha_1 t} + f_2 e^{\alpha_2 t} + f_3 e^{\alpha_3 t}, \tag{B2}$$

and

$$M_z(t) = m_z^{ss} + m_1 e^{\alpha_1 t} + m_2 e^{\alpha_2 t} + m_3 e^{\alpha_3 t}, \tag{B3}$$

where

$$\begin{cases} g_x^{ss} = \dfrac{M_z^0 R_1 R_2 \omega_1}{R_1[R_2^2 + (\Delta\omega)^2] + \omega_1^2 R_2} \\ g_1 = \dfrac{\omega_1(R_2+\alpha_1)(R_1+\alpha_1)}{\alpha_1(\alpha_1-\alpha_2)(\alpha_1-\alpha_3)} \\ g_2 = \dfrac{\omega_1(R_2+\alpha_2)(R_1+\alpha_2)}{\alpha_2(\alpha_2-\alpha_1)(\alpha_2-\alpha_3)} \\ g_3 = \dfrac{\omega_1(R_2+\alpha_3)(R_1+\alpha_3)}{\alpha_3(\alpha_3-\alpha_1)(\alpha_3-\alpha_2)} \end{cases}, \tag{B4}$$

$$\begin{cases} f_x^{ss} = \dfrac{M_z^0 R_1 \Delta\omega\omega_1}{R_1[R_2^2 + (\Delta\omega)^2] + \omega_1^2 R_2} \\ f_1 = \dfrac{\omega_1\Delta\omega(R_1+\alpha_1)}{\alpha_1(\alpha_1-\alpha_2)(\alpha_1-\alpha_3)} \\ f_2 = \dfrac{\omega_1\Delta\omega(R_1+\alpha_2)}{\alpha_2(\alpha_2-\alpha_1)(\alpha_2-\alpha_3)} \\ f_3 = \dfrac{\omega_1\Delta\omega(R_1+\alpha_3)}{\alpha_3(\alpha_3-\alpha_1)(\alpha_3-\alpha_2)} \end{cases}, \tag{B5}$$

and

$$\begin{cases} m_z^{ss} = \dfrac{M_z^0 R_1[R_2^2 + (\Delta\omega)^2]}{R_1[R_2^2 + (\Delta\omega)^2] + \omega_1^2 R_2} \\ m_1 = \dfrac{[(R_2+\alpha_1)^2 + (\Delta\omega)^2](R_1+\alpha_1)}{\alpha_1(\alpha_1-\alpha_2)(\alpha_1-\alpha_3)} \\ m_2 = \dfrac{[(R_2+\alpha_2)^2 + (\Delta\omega)^2](R_1+\alpha_2)}{\alpha_2(\alpha_2-\alpha_1)(\alpha_2-\alpha_3)} \\ m_3 = \dfrac{[(R_2+\alpha_3)^2 + (\Delta\omega)^2](R_1+\alpha_3)}{\alpha_3(\alpha_3-\alpha_1)(\alpha_3-\alpha_2)} \end{cases}. \tag{B6}$$

The exponential coefficients in Eqs. (B1), (B2) and (B3) are given by

$$\begin{cases} \alpha_1 = \dfrac{-(2R_2+R_1)}{3} + A + B \\ \alpha_2 = \dfrac{-(2R_2+R_1)}{3} - \dfrac{A+B}{2} + i\sqrt{3}\dfrac{A-B}{2} \\ \alpha_3 = \dfrac{-(2R_2+R_1)}{3} - \dfrac{A+B}{2} - i\sqrt{3}\dfrac{A-B}{2} \end{cases}, \tag{B7}$$

where

$$i = \sqrt{-1}, A = \left[-\frac{b}{2} + \sqrt{c}\right]^{\frac{1}{3}}, B = \left[-\frac{b}{2} - \sqrt{c}\right]^{\frac{1}{3}}, \tag{B8}$$

$$b = \frac{1}{27}(R_1 - R_2)\left[2(R_1 - R_2)^2 + 18(\Delta\omega)^2 - 9\omega_1^2\right], \tag{B9}$$

and

$$c = \frac{1}{27}\left\{[(\Delta\omega)^2 + \omega_1^2]^3 + (R_1 - R_2)^2 \times \left(2(\Delta\omega)^2\left[2(\Delta\omega)^2 + (R_1 - R_2)^2\right] - \omega_1^2\left[\frac{\omega_1^2}{4} + 5(\Delta\omega)^2\right]\right)\right\}. \tag{B10}$$

## References


[1] Ward K, Aletras A, Balaban R. A new class of contrast agents for MRI based on proton chemical exchange dependent saturation transfer (CEST). J Magn Reson 2000;143:79–87.

[2] Goffeney N, Bulte JW, Duyn J, Bryant LH, van Zijl PCM. Sensitive NMR detection of cationic-polymer-based gene delivery systems using saturation transfer via proton exchange. J Am Chem Soc 2001;123: 8628–9.

[3] Aime S, Barge A, Delli Castelli D, Fedeli F, Mortillaro A, Nielsen FU, Terreno E. Paramagnetic Lanthanide (III) complexes as pH-sensitive chemical exchange saturation transfer (CEST) contrast agents for MRI applications. Magn Reson Med 2002;47:639–48.

[4] Snoussi K, Bulte JWM, Gueron M, van Zijl PCM. Sensitive CEST agents based on nucleic acid imino proton exchange: detection of poly (rU) and of a dendrimer-poly(rU) model for nucleic acid delivery and pharmacology. Magn Reson Med 2003;49:998–1005.

[5] Zhou J, Lal B, Wilson DA, Laterra J, van Zijl PCM. Amide proton transfer (APT) contrast for imaging of brain tumors. Magn Reson Med 2003;50:1120–6.

[6] Sun PZ, Murata Y, Lu J, Wang X, Lo EH, Sorensen AG. Relaxation-compensated fast multislice amide proton transfer (APT) imaging of acute ischemic stroke. Magn Reson Med 2008;59:1175–82.

[7] Sun PZ. Simultaneous determination of labile proton concentration and exchange rate utilizing optimal RF power: radio frequency power (RFP) dependence of chemical exchange saturation transfer (CEST) MRI. J Magn Reson 2010;202:155–61.

[8] Woessner DE, Zhang S, Merritt ME, Sherry AD. Numerical solution of the Bloch equations provides insights into the optimum design of PARACEST agents for MRI. Magn Reson Med 2005;53:790–9.

[9] Mulkern RV, Williams ML. The general solution to the Bloch equation with constant rf and relaxation terms: application to saturation and slice selection. Med Phys 1993;20:5–13.

[10] Roell SA, Dreher W, Leibfritz D. A general solution of the standard magnetization transfer model. J Magn Reson 1998;132:96–101.

[11] Madhu PK, Kumar A. Direct cartesian-space solutions of generalized Bloch equations in the rotating frame. J Magn Reson A 1995;114: 201–11.

[12] Roberts JD. The Bloch equations. How to have fun calculating what happens in NMR experiments with a personal computer. Concepts Magn Reson 1991;3:27–45.

[13] Abragram A. Principles of nuclear magnetic resonance. London: Oxford University Press; 1961. p. 45–6.

[14] Pedersen JB. Theory of transient effects in time resolved ESR spectroscopy. J Chem Phys 1973;59:2656–67.

[15] Slichter CP. Principles of magnetic resonance. New York: Springer Verlag; 1989. p. 35–6.

[16] Haacke EM, Brown RW, Thompson MR, Venkatesan R. Magnetic resonance imaging: physical principles and sequence design. New York: John Wiley & Sons, Inc.; 1999. p. 51–64.

[17] Sun PZ, van Zijl PCM, Zhou J. Optimization of the irradiation power in chemical exchange dependent saturation transfer experiments. J Magn Reson 2005;175:193–200.

[18] Shampine LF, Watts HA, Davenport SM. Solving nonstiff ordinary differential equations – the state of the art. SIAM Rev 1976;18: 376–411.

[19] Higham NJ. The scaling and squaring method for the matrix exponential revisited. SIAM J Matrix Anal Appl 2005;26:1179–93.

[20] Smith SA, Farrell JAD, Jones CK, Reich DS, Calabresi PA, van Zijl PCM. Pulsed magnetization transfer imaging with body coil transmission at 3 Tesla: feasibility and application. Magn Reson Med 2006;56:866–75.